Article

Discovery Medicine 2026; 38(209): 1862–1874
https://doi.org/10.24976/Discov.Med.202638209.145

Proteomic Analysis of Urinary Exosomal S100 Proteins Identifies S100A6 as a Non-Invasive Biomarker for Small Cell Lung Cancer in Male Patients

Weiwei Wang[1,†], Na Liu[2,3,†], Shanshan Wang[1], Alifeila·Aili[1], Lei Pan[1,*], Man Zhang[2,3,*]

[1]Department of Respiratory and Critical Care, Beijing Shijitan Hospital, Capital Medical University, 100038 Beijing, China
[2]Clinical Laboratory Medicine, Beijing Shijitan Hospital, Capital Medical University, 100038 Beijing, China
[3]Beijing Key Laboratory of Urinary Cellular Molecular Diagnostics, 100038 Beijing, China
*Correspondence: panlei@bjsjth.cn (Lei Pan); zhangman@bjsjth.cn (Man Zhang)
[†]These authors contributed equally.
Submitted: 26 February 2026 Revised: 17 April 2026 Accepted: 24 April 2026 Published: 20 June 2026

Background: Small cell lung cancer (SCLC) has a poor prognosis, creating a need for non-invasive diagnostic biomarkers. Urinary exosomes, enriched with tumor-derived biomolecules, offer a non-invasive avenue for biomarker discovery. This study investigates the expression profiles of S100A proteins in urinary exosomes for SCLC detection.

Methods: Urinary exosomes were isolated from 26 male SCLC patients and 26 male healthy controls. The cohort was randomly divided into discovery and validation sets of 13 patients and 13 controls each. Proteomic profiling using data-independent acquisition mass spectrometry identified differentially expressed S100A proteins. Age- and sex-specific patterns were examined in 210 healthy individuals. Key findings were validated by parallel reaction monitoring.

Results: SCLC exosomes showed significant downregulation of S100A2/A6/A8/A9/A11/A16 (fold change >1.5, $p < 0.05$) and specific upregulation of S100A7 ($p < 0.001$). S100A6 demonstrated superior diagnostic performance with area under the curve (AUC) = 0.98 (95% CI: 0.94–1.00) in the discovery cohort and maintained AUC = 0.86 (95% CI: 0.71–1.00) in the validation cohort. Protein interaction analysis uncovered potential interactions among S100A members, particularly between S100A8/A16 ($r = 0.86$, $p < 0.001$). Age-sex stratification revealed significant population heterogeneity in the abundance of S100A2/A7/A8/A9/A16 ($p < 0.001$), whereas S100A6 abundance remained stable across subgroups.

Conclusion: Urinary exosomal S100 proteins, particularly the stable and high-performing S100A6, serve as promising non-invasive biomarkers for male patients with SCLC. The identified population-specific abundance patterns provide a basis for personalized diagnostics.

Keywords: small cell lung cancer; urinary exosomes; S100 proteins; S100A6; biomarker; data-independent acquisition mass spectrometry

Introduction

Small cell lung cancer (SCLC) is a neuroendocrine malignancy known for its aggressiveness, rapid proliferation, early dissemination, and poor prognosis, particularly in the extensive-stage form. Although significant advancements have been made in multimodal therapy, the 5-year survival rate remains below 7%, largely due to delayed diagnosis and limited monitoring tools [1,2]. Current diagnostic practices rely on imaging and tissue biopsies, which are invasive and unsuitable for real-time disease tracking. Available serum biomarkers such as neuron-specific enolase (NSE) and Progastrin-Releasing Peptide (ProGRP) offer limited sensitivity and specificity, highlighting an unmet need for non-invasive, robust, and reproducible diagnostic alternatives [3].

The S100 protein family is a well-characterized subgroup of EF-hand calcium-binding proteins, consisting of 25 functionally diverse members: the S100A1–S100A16 subfamily, encoded by genes clustered at the chromosome 1q21 locus, and additional non-A members (S100B, S100G, S100P, S100Z) encoded by genes at other chromosomal loci. The S100 family is involved in several biological processes in cancer and other physiological contexts through interactions with various signaling proteins. Notably, S100 proteins exert distinct functions through subtype-specific mechanisms across different forms of lung cancer [4,5]. Aberrant expression of S100 proteins has been implicated in multiple cancers, including lung, breast, bladder, and cervical carcinomas. However, their role in SCLC, particularly within exosomes, remains underexplored [4,6–8].

Urinary exosomes are extracellular vesicles enriched in disease-relevant biomolecules. They represent an attractive platform for liquid biopsy due to their stability, accessibility, and potential to reflect the systemic tumor microenvironment. While proteomic profiling of exosomes has gained traction in oncology, a critical gap remains in characterizing exosomal protein signatures specific to SCLC, particularly the role of the S100 family within exosomal compartments [9].

This study addresses that gap by performing a comprehensive urinary exosome proteomic analysis using data-independent acquisition mass spectrometry (DIA-MS) to interrogate S100 protein abundance in SCLC patients versus healthy controls. We focused on the S100A family of proteins due to their consistent differential abundance in our dataset and their known biological relevance in tumor biology. Among the identified candidates, S100A6 emerged as a demographically stable and diagnostically robust marker, showing strong discriminatory power and minimal variability across age and sex subgroups. By systematically evaluating the abundance, interaction, and diagnostic utility of S100 proteins in urinary exosomes, our study addresses a significant gap in SCLC biomarker research and introduces a promising direction for non-invasive diagnostics. By focusing on this protein family, our work not only uncovers new diagnostic opportunities but also lays the groundwork for mechanistic insights into SCLC exosome-mediated tumor biology.

Methods

Study Cohort

Prior to the study initiation, informed consent was obtained from all study participants before being enrolled. The study adhered to the standards outlined in the Declaration of Helsinki and was approved by the Ethics Committee of Beijing Shijitan Hospital (No. 5, 2017). The study cohort comprised small cell lung cancer (SCLC) patients and healthy controls (HC) recruited from Beijing Shijitan Hospital, Capital Medical University between January 2019 and January 2024. SCLC was pathologically confirmed by two senior pathologists through histopathological examination, and immunohistochemical detection of chromogranin A, synaptophysin, and CD56, to ensure accurate diagnosis. Clinical assessments included tumor staging using the Veterans Administration Lung Study Group (VALSG) system and Eastern Cooperative Oncology Group (ECOG) performance status evaluation.

Exclusion criteria for SCLC patients were as follows: (1) presence of other histopathological types of lung cancer or secondary lung tumors; (2) concurrent autoimmune diseases, severe cardiovascular diseases, diabetes, or chronic liver or kidney diseases; (3) acute urinary tract infection or hematuria; (4) prior treatment with chemotherapy, radiotherapy, targeted therapy, or immunotherapy before sample collection; and (5) urinary albumin/creatinine ratio $\leq$30 mg/g. Exclusion criteria for healthy controls were as follows: (1) history of malignant tumors; (2) presence of autoimmune diseases, cardiovascular diseases, diabetes, or chronic liver or kidney diseases; (3) acute urinary tract infection or hematuria; (4) abnormal routine blood or urine test results; and (5) urinary albumin/creatinine ratio $\leq$30 mg/g.

This study included two distinct cohorts. The first cohort was designed to explore and validate changes in S100A proteins abundance in SCLC patients, and this included 26 male SCLC patients and 26 male healthy controls. A simple random sampling method was applied using the random number table function in SPSS 27.0 (Armonk, NY, USA) to randomly assign the cohort to the discovery set (13 patients and 13 healthy controls) and the validation set (13 patients and 13 healthy controls). The randomization process was performed by an independent statistician, and age and smoking history were assessed to confirm that no baseline differences existed between the two groups. The second cohort comprised healthy individuals stratified into seven age groups: 0–6, 7–14, 15–30, 31–44, 45–59, 60–79, and $>$80 years. Each group included 30 individuals, 15 males and 15 females. This cohort was specifically utilized for mass spectrometry analysis to investigate age- and sex-related variations in S100A proteins expression.

Isolation and Identification of Exosomes From Human Urine Samples

Midstream urine samples were collected from SCLC patients prior to chemoradiotherapy and from healthy controls. All collection procedures adhered to the standardized protocols established by our group previously [10]. All participants provided written informed consent prior to sample collection. Upon collection, urine samples were immediately processed or stored at –80 °C until further use.

To separate exosomes, urine samples were thawed at 37 °C and then centrifuged in steps. The first centrifugation step was performed in a Sorvall ST 8R centrifuge (Thermo Scientific, Waltham, MA, USA) and continued for 30 minutes, at 4 °C and 2000 $\times$g. After that, centrifugation of the supernatant was repeated for 45 minutes at 10,000 $\times$g and 4 °C to get rid of big vesicles. For supernatant filtration, a 0.45 µm polyethersulfone membrane (Millipore, Billerica, MA, USA, catalog number: R6BA09493) was used, and then was concentrated using a type 70 Ti rotor (Beckman Coulter, Brea, CA, USA) via ultracentrifugation for 70 minutes, at 100,000 $\times$g and 4 °C. The pellet was resuspended in 10 mL of ice-cold 1$\times$ PBS (pH 7.4) and ultracentrifuged again under the same conditions. The final exosome pellet was resuspended in 100 µL of PBS and stored at –80 °C. Three microliters (µL) from each sample were mixed to make composite samples for quality control. The following volumes were subsequently added to these aliquots: 20 µL for transmission electron microscopy (TEM) and Western blotting, and 10 µL for nanoparticle tracking analysis.

To analyze exosomal morphology, TEM was performed according to the exosome characterization protocols by the International Society for Extracellular Vesicles (ISEV). The experimental procedure involved applying 10 µL of purified extracellular vesicle suspension onto a copper mesh grid, followed by a 60-second incubation period. An absorbent paper was used to absorb the residual liquid. Uranyl acetate solution (10 µL, 2% solution) was added for 60 seconds to perform the negative staining, followed by removal of excess staining reagent. The prepared grid was air-dried at ambient temperature before being subjected to TEM analysis using a Hitachi HT-7700 system (Hitachi High-Tech, Tokyo, Japan) with an accelerating voltage of 100 kV. Morphological assessment was conducted by acquiring electron micrographs.

NTA analysis was performed using a ZetaVIEW TWIN instrument (Particle Metrix, Meerbusch, Germany) calibrated with 100 nm polystyrene beads. Samples were diluted with PBS to 1–5 $\times$ 10^8 particles/mL and measured at 25 °C; five technical replicates were acquired for each biological sample.

Western blotting was used to verify the expression of protein in the urine exosome. After lysis, equal protein amounts were separated on 12% Tris-HCl SDS-PAGE gels and transferred to PVDF membranes via a Trans-Blot Turbo system (Bio-Rad, CA, USA). Membranes were blocked at room temperature for 2 h with gentle shaking. CD9 primary antibody (Abcam, Cambridge, UK; catalog number: ab236630; 1:1000) was incubated overnight at 4 °C. After three 15-min washes in TBST, horseradish peroxidase-conjugated secondary antibody (Bioss, Beijing, China; anti-Rabbit IgG, Lot:158560; diluted by 1:2000) was applied for 2 h at room temperature. The target components were finally detected using enhanced chemiluminescence (ECL, Bio-Rad, cat. t#170–5061).

Proteomics Analysis of the Urinary Exosome

Protein Extraction

Exosomes were thawed immediately at 37 °C and lysed using 5 $\times$ radioimmunoprecipitation assay (RIPA) buffer. The mixture was thoroughly vortexed, followed by 30 minutes of incubation on ice with intermittent mixing. BCA assay was used to determine protein concentration. The BCA working reagent was mixed with a 5 µL aliquot of each lysate, and the total protein yield was calculated as the product of concentration and total lysate volume.

Protein Digestion, Desalination, and Library Construction

A 200 mM solution of dithiothreitol (DTT, Amresco, Solon, Ohio, USA; Lot: M109-5G) was used to reduce a 200 µg aliquot of extracted proteins from each sample, which was then incubated at 37 °C for 1 hour. Then, 50 mM ammonium bicarbonate (ABC, Sigma-Aldrich, St. Louis, Missouri, USA; Lot: A6141-500G) buffer was used to dilute the sample fourfold, followed by the addition of trypsin (trypsin-to-protein ratio of 1:50) and incubation overnight at 37 °C. 50 µL of 0.1% formic acid (FA, Sigma-Aldrich, St. Louis, Missouri, USA; Lot: T79708) was added to stop the digestion. A C18 column was utilized to desalt the peptides, then washed with 100% acetonitrile (ACN, J.T.Baker, Phillipsburg, New Jersey, USA; Lot: 34851), and eluted with 70% ACN. The combined eluents were then lyophilized and stored at –80 °C until further analysis.

For peptide fractionation, samples were separated on a Waters BEH C18 column (4.6 $\times$ 250 mm, 5 µm) using an EASY-nLC1200 UHPLC system at 1 mL/min flow rate (column oven 50 °C). Mobile phases consisted of 2% ACN (pH 10.0, phase A) and 98% ACN (pH 10.0, phase B). A multi-step gradient was applied: 5% B (0–5 min), 8% B (5–35 min), 18% B (35–57 min), 32% B (57–59 min), 95% B (59–63 min), and 5% B (63–67 min). Eluates monitored at 214 nm were collected at 1-min intervals and combined into six fractions. After vacuum drying, fractions were reconstituted in 0.1% FA and spiked with iRT standard peptides (Biognosys, Schlieren, Zurich, Switzerland).

The spectral library was constructed in data-dependent acquisition (DDA) mode using an Orbitrap Eclipse mass spectrometer (Thermo Fisher Scientific, Waltham, Massachusetts, USA) coupled to an EASY-nLC1200 system. Tryptic peptides were loaded onto a 25-cm analytical column (100 µm ID, ReproSil-Pur C18-AQ 1.5-µm beads) and separated with a 65-min gradient: 6–12% B (0–13 min), 12–30% B (13–46 min), 30–40% B (46–53 min), 95% B (53–54 min), 95% B (54–64 min), and 6% B (64–65 min) at 300 nL/min (solvent A: 0.1% FA; B: 80% ACN/0.1% FA). MS1 spectra were acquired at a resolution of 120,000 at m/z 200 (350–1500 m/z) with an automatic gain control (AGC) target of 3 $\times$ 10^6 and a maximum injection time of 50 ms. Following each full MS1 scan, the 40 most intense precursor ions were selected for tandem MS analysis with an isolation width of 1.6 m/z. MS2 spectra were acquired at 15,000 resolution at m/z 200 with a normalized collision energy of 33%, an AGC target of 5 $\times$ 10^4, and a maximum injection time of 22 ms. Precursor dynamic exclusion was enabled with a duration of 16 s to minimize redundant acquisition of the same precursor.

Liquid Chromatography-Tandem Mass Spectrometry (LC-MS/MS) Data-Independent Acquisition (DIA)

For quantitative proteomic analysis, the same LC configurations and solvent systems were employed, consisting of an EASY-nLC1200 system (Thermo Fisher Scientific, Waltham, MA, USA) coupled with a 25-cm C18 column (Beijing Qinglian Biotech Co., Ltd., Beijing, China). Peptides were separated using an identical 65-min gradient as described for library generation. DIA was performed on the Orbitrap Eclipse mass spectrometer with consistent MS parameters: MS1 at 120,000 resolution (350–1500 m/z, 50 ms max IT) and MS2 scans at 15,000 resolution (200–2000 m/z, 22 ms max IT) using 33% HCD energy. Forty-

two variable isolation windows covering the 350–1500 m/z range were implemented for comprehensive peptide fragmentation.

Protein Identification and Quantification

The Spectronaut software (version 16.0; Biognosys, Schlieren, Zurich, Switzerland) was used to process mass spectrometry data from fractionated pools (DDA MS data, 6 fractions) and single-shot samples (DIA MS data) to construct a hybrid spectral library. The library was used to search MS data from single-shot samples for protein identification and quantification. We searched the human UniProt reference proteome (20,361 target sequences, retrieved on 2022-03-17) with carbamidomethylation as a fixed modification and acetylation of the protein N-terminus and oxidation of methionines as variable modifications. A trypsin/P cleavage rule was used, which allowed for up to two miscleavages and peptide lengths of 7 to 52 amino acids. The "Local Normalization" technique in Spectronaut was used to make protein intensities the same. Each peptide had to have at least three fragments and no more than six fragments, to make a spectral library. A false discovery rate (FDR) of 1% was used for proteins and precursors, and only proteins that cleared the filter were reported.

Functional Analysis of Proteins and Differentially Expressed Proteins (DEPs)

Raw data were standardized using the median method to minimize experimental variation. Data with more than 50% missing values were removed, and the remaining missing values were imputed using the K-nearest neighbors (KNN) method. DEPs were identified based on an average fold change >1.2 and an adjusted p-value < 0.05; then, considering the disease characteristics of SCLC, a more stringent threshold of fold change >1.5 and $p < 0.05$ was used as the final screening criterion for differential S100A proteins to improve the specificity of candidate biomarkers. Functional analysis of proteins and DEPs was conducted using Gene Ontology (GO) terms obtained from the GO database, with proteins categorized according to molecular function, biological process, and cellular component. In addition, protein–protein interaction networks were predicted using the STRING database.

Protein Validation by Parallel Reaction Monitoring (PRM)

Protein Extraction and Digestion

Exosomal proteins were isolated and extracted following the standardized protein extraction procedure described in the preceding urinary exosome proteomics analysis section. For proteomic analysis, 1 mM dithiothreitol (DTT, 37 °C, 1 h) was used to reduce 60 µg of protein from each sample, and iodoacetamide (room temperature, dark, 1 h) was used for alkylation. Enzymatic digestion was performed using Trypsin Gold (Promega, V5111) at a 1:50 (w/w) enzyme-to-substrate ratio in 50 mM ammonium bicarbonate buffer (37 °C, 16 h). Digested peptides were desalted using C18 cartridges (Waters), dried by vacuum centrifugation, and stored at –80 °C. A pooled reference sample was generated by combining equal aliquots from individual digests for downstream fractionation.

HPLC Fractionation

A Rigol L3000 HPLC (RIGOL Technologies, Inc., Beijing, China) with a C18 column (Waters BEH C18 4.6 $\times$ 250 mm, 5 µm) was used to fractionate pooled peptides. The column oven was set to 50 °C and the flow rate was 0.7 mL/min. To make a gradient elution, we employed mobile phases A (100% water, 0.1% formic acid) and B (100% acetonitrile, 0.1% formic acid). The solvent gradient was set as follows: 8% B for 0 minutes, 12% B for 5 minutes, 30% B for 30 minutes, 40% B for 9 minutes, 95% B for 1 minute, and 95% for 15 minutes. The eluates were monitored at UV 214 nm, collected at one tube per minute, and finally combined into 3 fractions. All fractions were dried under vacuum and reconstituted in 0.1% (v/v) formic acid (FA) in water.

LC-MS/MS Analysis-DDA Mode

Shotgun proteomics analyses were performed using a Q Exactive HF-X mass spectrometer (Thermo Fisher Scientific, Waltham, Massachusetts, USA) in data-dependent acquisition mode. A 1 µg peptide sample was loaded onto a custom-made C18 Nano-Trap column (2 cm $\times$ 100 µm, 3 µm). Peptide separation was carried out on an analytical column (25 cm $\times$ 75 µm, 100 Å) using an 80-minute linear gradient from 0 to 95% solvent B, with a flow rate of 600 nL/min. The gradient profile was as follows: 8% B at 0 min, 8–12% B at 7 min, 12–30% B at 48 min, 30–40% B at 10 min, and 40–95% B at 15 min. Mass spectrometry data were acquired using a Nanospray Flex™ (NSI) ion source, with the ion spray voltage set to 2.4 kV and the ion transfer tube temperature set to 275 °C. The instrument was operated in DDA mode with the following parameters: full MS1 scan range was set to m/z 350–1500, with a resolution of 120,000 at m/z 200, a C-trap maximum capacity (automatic gain control, AGC target) of 3×10^6, and a maximum C-trap injection time of 80 ms. The top 40 precursor ions with the highest ion intensity in each full MS1 scan were selected for fragmentation via higher-energy collisional dissociation (HCD) for MS2 detection. The MS2 parameters were set as follows: resolution of 15,000 at m/z 200, a C-trap maximum capacity (AGC target) of 5×10^4, a maximum C-trap injection time of 45 ms, a normalized collision energy of 27%, an intensity threshold for triggering MS2 of 1.1×10^4, and a dynamic exclusion duration of 16 s.

LC-MS/MS Analysis-PRM Mode

The reconstituted sample was analyzed using an EASY nLC 1200 ultra-high-pressure system (Thermo Fisher Scientific, Waltham, Massachusetts, USA) coupled to a Q Exactive HF-X mass spectrometer operating in PRM mode. The sample was reconstituted in 0.1% formic acid prior to analysis. Chromatographic conditions were identical to the DDA method. PRM acquisition parameters were set in this order: MS1 resolution at 60,000, MS2 resolution at 60,000, m/z range 350–1500, full scan AGC target of 3×10^6, injection time of 80 ms, normalized collision energy of 27%, PRM target value of 5×10^4, and maximum injection time of 45 ms.

Data Analysis

Unique peptides (7–25 amino acids; no missed cleavages, methionine oxidation, or N-terminal modifications) were selected from the DDA data based on spectral quality. Skyline 22.2 was used for spectral library creation and analysis. Database searching allowed for trypsin digestion (cleavage before proline), up to two missed cleavages, cysteine carbamidomethylation (fixed), and N-terminal acetylation/methionine oxidation (variable modifications). Precursor charges (2, 3, 4), product ion charges (1, 2), and b/y/a ions were considered; fragment ion selection started from the third to the last amino acid. The mass error tolerance was 0.02 Da. A 1% FDR was applied for proteins and precursors, and only those that passed the filter were reported.

Statistical Analysis

SPSS 27.0 and GraphPad Prism 9.5.1 were used for the statistical analyses and data were presented as mean ± standard deviation or median with interquartile range. Normality was assessed using the Shapiro–Wilk test. Comparative analyses between groups utilized *t*-tests for normally distributed continuous variables, Mann-Whitney U tests for non-normally distributed data, and Chi-squared tests for categorical variables. Correlation analyses were conducted using Pearson's correlation for normally distributed data and Spearman's rank correlation for non-normally distributed data. Diagnostic performance was evaluated through receiver operating characteristic (ROC) curve analysis, with statistical significance defined as $p < 0.05$.

Results

Patient Demographics and Clinical Characteristics

The study comprised 26 male SCLC patients and 26 age- and gender-matched healthy controls (Table 1). There were no significant differences in age (65.2 ± 9.3 vs. 65.6 ± 9.0 years, $p = 0.89$) or smoking history (non-smokers: 31%; ever-smokers: 69%, $p = 1.00$) between groups. Among SCLC patients, 81% (21/26) were diagnosed at the extensive stage, and 85% (22/26) exhibited an Eastern Cooperative Oncology Group (ECOG) performance status of 0–1. Serum neuron-specific enolase (NSE) levels were significantly elevated in patients compared to controls (median [IQR]: 48.96 [28.98–99.78] vs. 10.84 [9.27–13.90] ng/mL, $p < 0.0001$). The study workflow is shown in details in Fig. 1.

Urinary Exosomes Characterization in SCLC

TEM was used to confirm the existence of exosomes in the urine samples of SCLC patients. The following applied techniques allowed confirmation of the alignment of exosome morphology and dimensions with established characteristics. TEM analysis confirmed the characteristic vesicular morphology of exosomes, revealing spherical bilayer membrane structures (Fig. 2A). Furthermore, NTA revealed that the average diameter of the isolated exosomes was 154.1 nm (Fig. 2B). To further verify the successful isolation of exosomes, western blot analysis was performed to examine the expression of the exosomal surface marker CD9 (Fig. 2C). The results demonstrated that CD9 was detectable in exosomal samples extracted from both the SCLC patient group and HC group. Taken together, these findings confirm the successful isolation and identification of urinary exosomes.

S100A Proteins Identification in Urinary Exosomes

Using DIA mass spectrometry, we profiled the urinary exosomal proteomes of 13 patients with SCLC and 13 healthy controls, with a particular emphasis on the S100A proteins. Our analysis detected several S100 family members in both groups, including S100A2, S100A6, S100A7, S100A8, S100A9, S100A11, and S100A16. A heatmap illustrating the hierarchical clustering of these S100A proteins is presented in Fig. 3A. GO analysis was conducted for these seven proteins, with results displayed in Fig. 3B. Additionally, protein–protein interaction networks among these S100 members were predicted using the STRING database, as shown in Fig. 3C.

S100 Family Members Differential Abundance Expression Analysis

Quantitative analysis of the DIA data revealed distinct expression profiles of S100 proteins between the two groups. Notably, S100A2, S100A6, S100A7, S100A8, S100A9, S100A11, and S100A16 showed significant differential expression (fold change >1.5, $p < 0.05$). Among these, the levels of S100A2, S100A6, S100A8, S100A9, S100A11, and S100A16 were significantly lower in the SCLC group than in the healthy controls ($p < 0.01$; Fig. 4A,B,D–G). In contrast, S100A7 was the only protein that exhibited a significant upregulation in SCLC patients ($p < 0.001$; Fig. 4C).

Table 1. Demographics of SCLC patients and healthy control subjects.

	SCLC patient (n = 26)	healthy control (n = 26)	Test statistic	p
Age	65.2 ± 9.3	65.6 ± 9.0	t = 0.123	p = 0.89
Gender				/
Female	0 (0%)	0 (0%)		
Male	26 (100%)	26 (100%)		
Smoking habit			χ^2 = 0.000	p = 1.00
Nonsmoker	8 (31%)	8 (31%)		
Ever smoker	18 (69%)	18 (69%)		
Clinical stage				
Limited stage	5 (19%)			
Extended stage	21 (81%)			
ECOG				
0–1	22 (85%)			
≥2	4 (15%)			
NSE (ng/mL)	48.96 (28.98∼99.78)	10.84 (9.27∼13.90)	Z = –5.124	p < 0.0001

SCLC, Small cell lung cancer; ECOG, Eastern Cooperative Oncology Group; NSE, neuron-specific enolase.

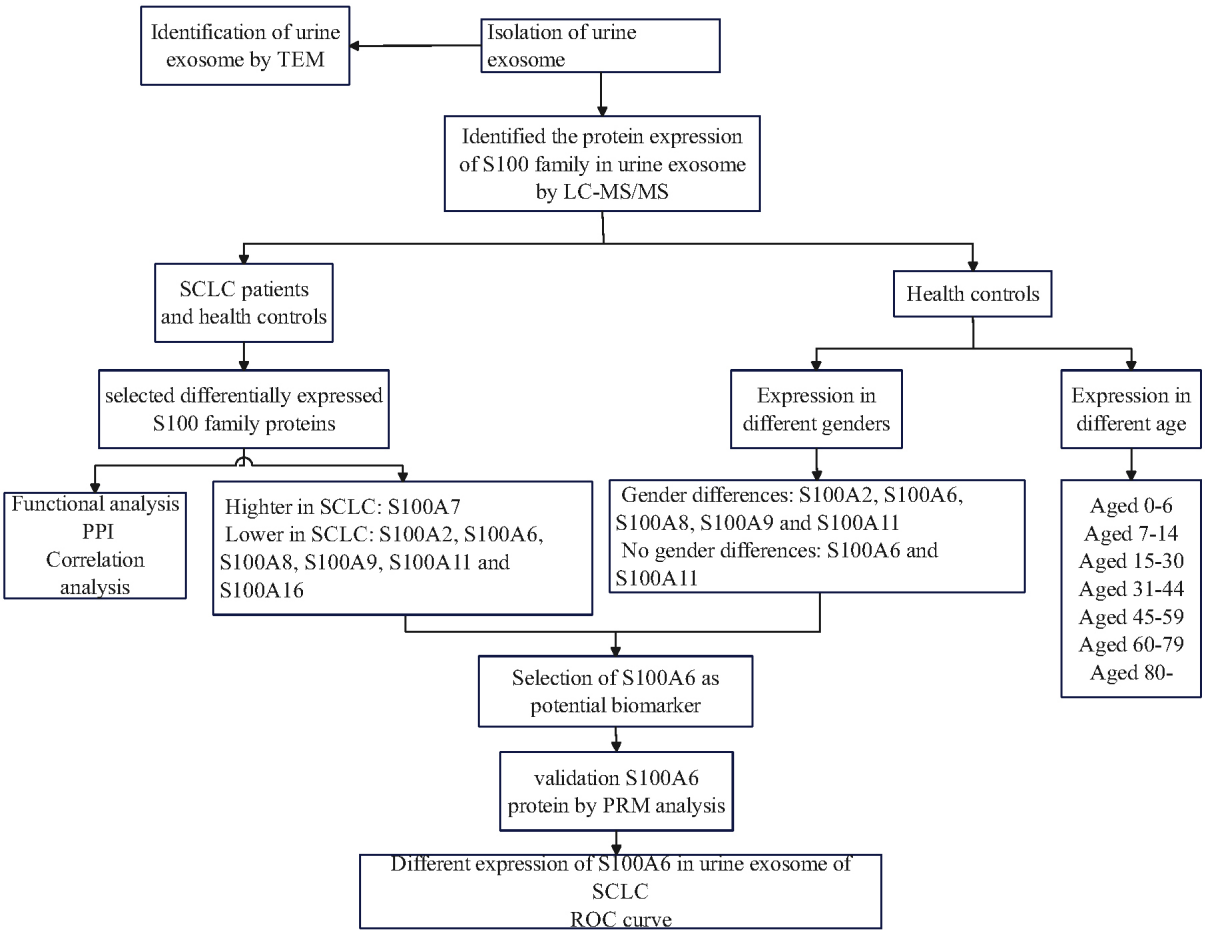

Fig. 1. Comprehensive workflow of S100 protein analysis in urinary exosomes from SCLC patients. SCLC, Small cell lung cancer.

Correlation Analysis of Different Abundance of S100 Proteins in Urinary Exosomes

Fig. 4H demonstrates the correlation analysis of S100 protein abundance, suggesting potential coordinated or antagonistic roles in SCLC-related pathways. Notably, S100A2 exhibited strong positive correlations with S100A8 (r = 0.79), S100A11 (r = 0.72), and S100A16 (r = 0.82) all at $p < 0.001$, indicating a possible synergistic involvement in inflammatory or oncogenic processes. Con-

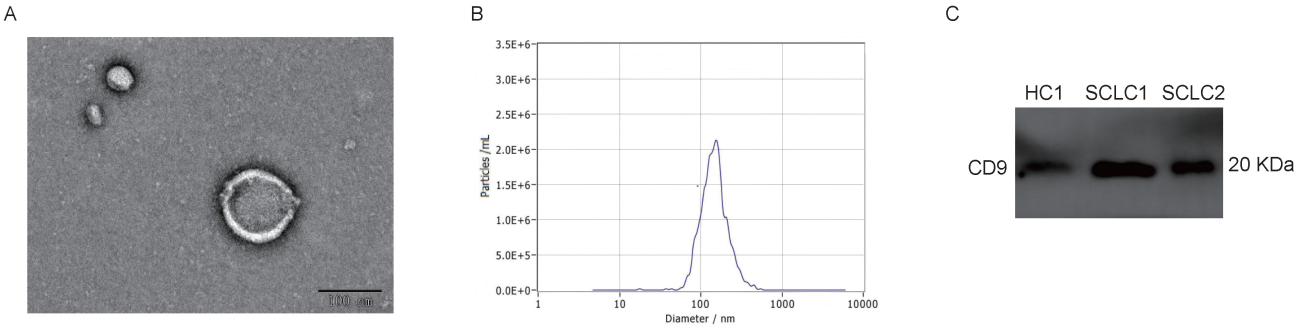

Fig. 2. Identification of urinary exosomes. (A) Transmission electron micrograph showing characteristic bilayer membrane structure of isolated urinary exosomes (scale bar: 100 nm). (B) Nanoparticle tracking analysis (NTA) displaying the size distribution of urinary exosomes, with an average diameter of 154.1 nm. (C) Western blot analysis identified the exosomal surface marker CD9 in exosome samples from both SCLC patients and HCs.

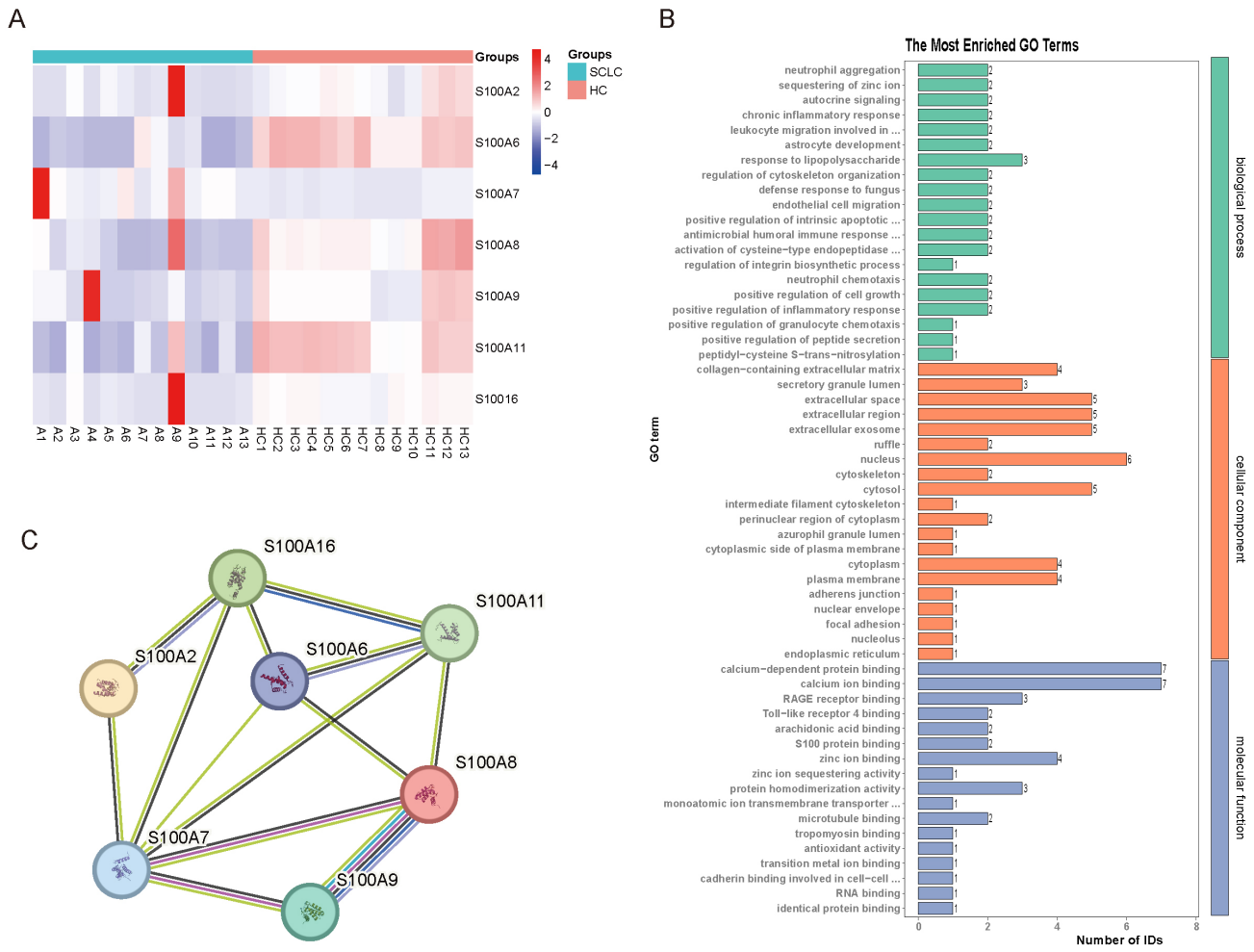

Fig. 3. Functional annotation and pathway analysis of S100 proteins. Comprehensive bioinformatics analysis of S100 proteins. (A) Heatmap visualization of protein abundance patterns across SCLC and healthy control groups. (B) Gene Ontology (GO) enrichment analysis highlighting biological processes, cellular components, and molecular functions. (C) Clustering analysis of differentially expressed proteins.

versely, S100A6 displayed divergent associations, showing a negative correlation with S100A7 ($r = –0.63$, $p < 0.001$), yet positive correlations with S100A8 ($r = 0.63$, $p < 0.001$), S100A11 ($r = 0.84$, $p < 0.001$) and S100A16 ($r = 0.64$, $p < 0.001$), implying context-dependent regulatory mechanisms. The robust correlation between S100A8 and

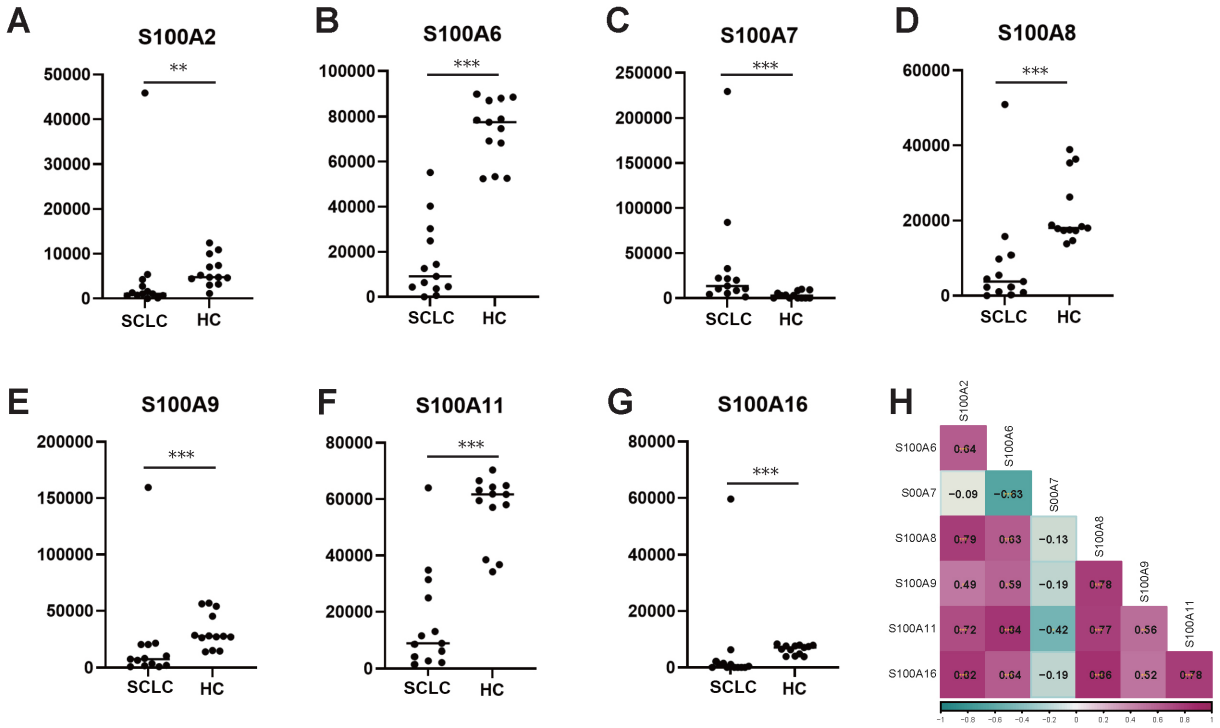

Fig. 4. Differential abundance and correlation analysis of S100A proteins in SCLC. Comparative protein abundance analysis of S100 family members between SCLC patients and healthy controls (SCLC = 13, HC = 13). (A–G) Quantitative representation of protein abundance levels for S100A2, S100A6, S100A7, S100A8, S100A9, S100A11, and S100A16. (H) Correlation matrix illustrating complex inter-protein relationships and statistical significance (**, $p < 0.01$; ***, $p < 0.001$).

S100A16 (r = 0.86, $p < 0.001$) further underscores their potential as co-regulated biomarkers in urinary exosomes.

Changes in the Abundance of S100 Proteins in Urinary Exosomes in Different Age and Sex Groups

The study investigated the abundance patterns of S100 proteins (S100A2, S100A6, S100A7, S100A8, S100A9, S100A11, and S100A16) in healthy individuals across different age groups (Fig. 5A–G). Quantitative analysis revealed sex differences in five urinary S100 proteins (S100A2, S100A7, S100A8, S100A9, and S100A16), while S100A6 and S100A11 exhibited no sex-dependent variations (Fig. 5H). Notably, S100A6, characterized by its stable abundance profile unaffected by sex and distinct age-related trends, was prioritized for further investigation. Therefore, subsequent studies will focus on validating the role of S100A6 in SCLC pathogenesis, with an emphasis on its potential as a robust biomarker for clinical diagnostics.

Validation of S100A6 Abundance Using PRM

To validate the differential abundance of S100A6 observed in the DIA analysis, a targeted mass spectrometry approach, PRM analysis, was utilized. The result confirmed the downregulation of S100A6 in urinary exosomes of SCLC patients compared to healthy controls ($p = 0.0018$) (Fig. 6A).

ROC Analysis

The ROC curve analysis was conducted in two independent phases to assess S100A6 as a diagnostic biomarker for SCLC. During the discovery phase, S100A6 demonstrated exceptional discriminative capacity with an AUC of 0.98 (95% confidence interval [CI]: 0.94–1.00, $p < 0.0001$), effectively distinguishing SCLC patients from healthy controls (Fig. 6B). This robust performance was subsequently validated in an independent cohort, where the biomarker maintained strong diagnostic accuracy with an AUC of 0.86 (95% CI: 0.71–1.00, $p < 0.01$). The consistent AUC values across both study phases suggest that S100A6 possesses reliable diagnostic potential for SCLC detection (Fig. 6C). In comparison, serum NSE, a conventional clinical biomarker for SCLC, yielded an AUC of 0.91 (95% CI: 0.821.00, $p <$ 0.0001) in the same overall cohort (Fig. 6D), further highlighting the non-invasive diagnostic utility of urinary exosomal S100A6.

Discussion

This study introduces a novel proteomic approach utilizing urinary exosomes to identify diagnostic biomarkers for SCLC, with a focused analysis of S100A proteins, which are known to regulate intracellular calcium homeostasis. Through proteomic profiling of urinary exosomes from male patients with SCLC, six members of the S100A

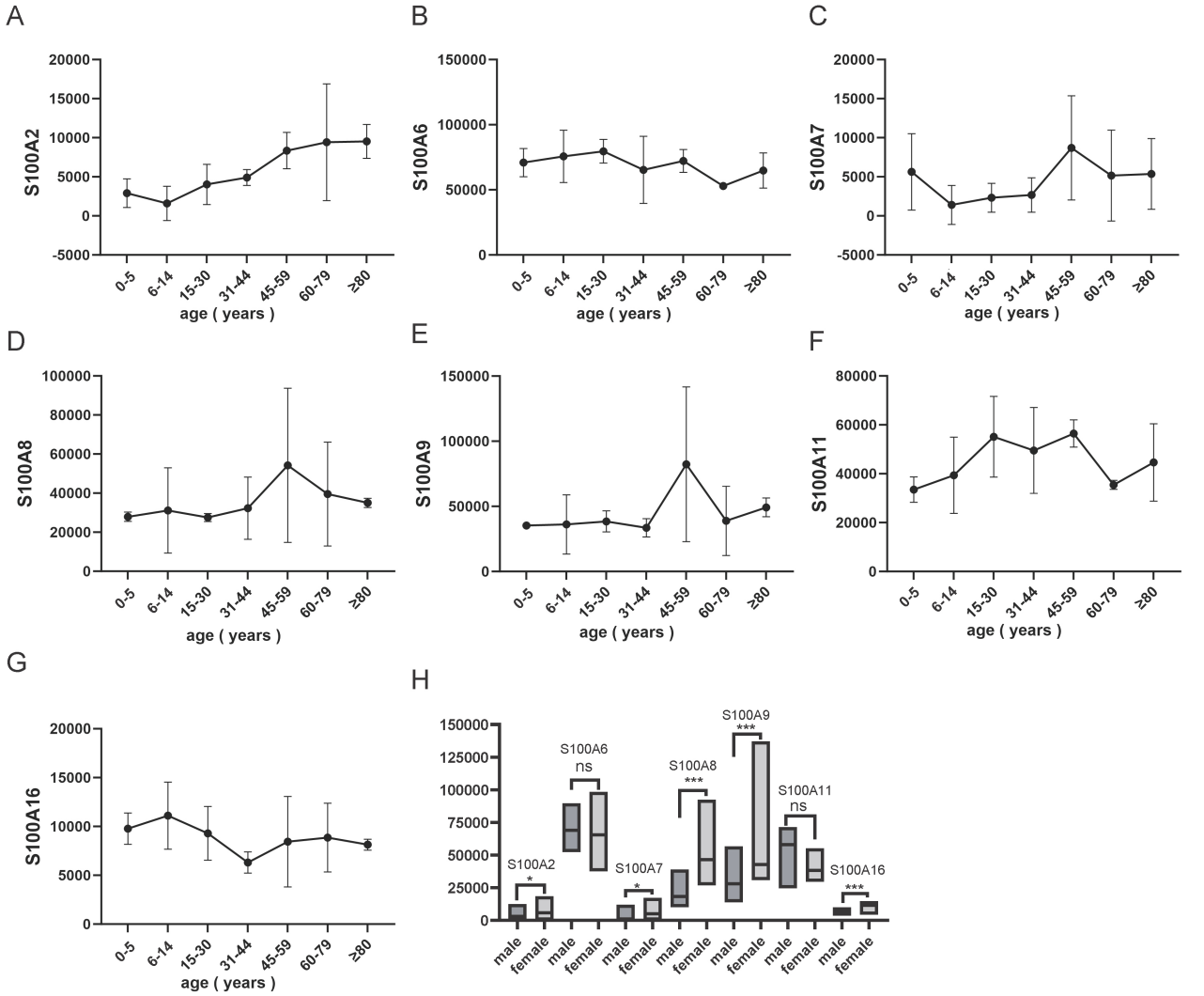

Fig. 5. Age- and gender-specific variations in S100 proteins abundance in urinary exosomes. Analysis of S100 protein abundance dynamics in healthy individuals (n = 210, divided into 7 age subgroups with 30 subjects per subgroup, 15 males and 15 females in each subgroup) stratified by age and gender. (A–G) Age-dependent trends in urinary exosomal protein levels: S100A2 (A), S100A6 (B), S100A7 (C), S100A8 (D), S100A9 (E), S100A11 (F), and S100A16 (G). (H) Gender-specific differences in total S100A proteins abundance, with statistical significance denoted (ns, not significant, *, $p < 0.05$, ***, $p < 0.001$).

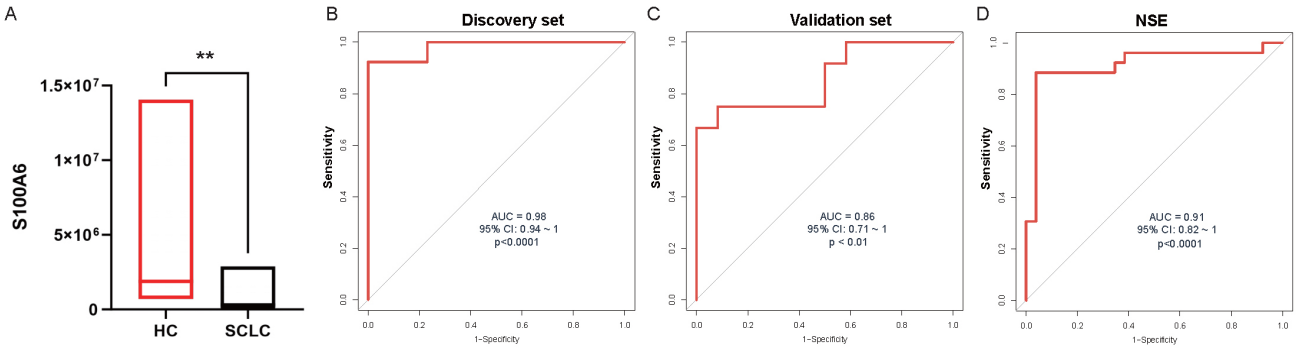

Fig. 6. Diagnostic performance of urinary exosome S100A6 protein biomarker. (A) Differential levels of S100A6 in urinary exosomes of SCLC patients within the validation cohort (SCLC = 13, HC = 13; **, $p < 0.01$). (B) ROC curve of S100A6 in the discovery cohort (SCLC = 13, HC = 13) with an AUC of 0.98. (C) ROC curve of S100A6 in the validation cohort (SCLC = 13, HC = 13) with an AUC of 0.86. (D) ROC curve analysis of serum NSE in the overall cohort (SCLC = 26, HC = 26) with an AUC of 0.91.

family, S100A2, S100A6, S100A8, S100A9, S100A11, and S100A16, were found to be significantly downregulated, while S100A7 was notably upregulated by 1.8-fold. Using DIA-MS and PRM validation, S100A6 was identified as a particularly promising diagnostic biomarker, showing excellent performance with an AUC of 0.98 in the discovery cohort and 0.86 in the validation cohort. These findings support the utility of S100A6 as a minimally invasive biomarker for the detection of SCLC.

The emphasis on the S100 family was motivated by their well-documented involvement in cancer biology, including their roles in immune regulation, epithelial mesenchymal transition (EMT), and inflammation [8,11,12]. Protein-protein interaction analysis using STRING revealed strong co-expression and functional connectivity among S100 members, suggesting a coordinated regulatory mechanism in the SCLC tumor microenvironment. S100A6, in particular, exhibited consistent detectability, demographic stability, and robust ROC performance, making it a clinically viable candidate for non-invasive diagnostics. This biomarker-focused strategy allowed the study to explore mechanistic relevance and clinical potential in depth, avoiding the dilution of findings that can result from broader, less targeted proteomic analyses.

Previous studies have shown that S100A6 expression is decreased in both glioma [13] and SCLC tissues [14], where it was shown to possess tumor-suppressive functions. Specifically, Li *et al*. [14] demonstrated that reduced S100A6 level in SCLC promoted tumor migration and invasion through the MAPK and TGF-β pathways. The results are in contrast with studies in ovarian cancer, where S100A6 was found to be upregulated and associated with increased proliferation [15]. Mechanistically, S100A6 may influence oxidative stress, apoptosis, and immune regulation, pathways often disrupted in SCLC. Its downregulation in tissues may reflect intrinsic tumor cell properties, while its decreased presence in urinary exosomes might suggest selective packaging processes within the tumor microenvironment. For example, reduced secretion of S100A6 into exosomes could impair extracellular matrix remodeling or immune evasion, as seen in stromal reprogramming processes [16]. This dual-level observation positions exosomal S100A6 not only as a surrogate for tissue expression but also as a potential indicator of systemic pathological activity, strengthening its role in liquid biopsy-based diagnostics.

Notably, this study distinguishes itself from prior research by using urinary exosomes as a non-invasive biomarker discovery, rather than relying on tumor tissues or serum. It also shows that S100A6 abundance remains stable across age and gender subgroups, expanding its clinical relevance. Some outliers in S100A6 abundance observed in the study may indicate poor prognosis, a phenomenon previously reported by He *et al*. [17].

In addition to S100A6, S100A2 was also significantly downregulated in urinary exosomes of SCLC patients, echoing Wang *et al*.'s [18] findings in SCLC tissue where the protein was undetectable, in contrast to its elevated expression in non-small cell lung cancer (NSCLC) subtypes and hepatocellular carcinoma [19]. This suppression may not only involve transcriptional regulation but also epigenetic mechanisms such as promoter hypermethylation, as reported in breast and bladder cancers [20,21]. Conversely, S100A2 is often upregulated in NSCLC subtypes like squamous cell carcinoma and adenocarcinoma, underscoring its context-dependent role: a tumor suppressor in SCLC but potentially oncogenic in NSCLC.

The study also reported elevated levels of S100A7 in urinary exosomes of SCLC patients, consistent with pan-cancer data from the Cancer Genome Atlas (TCGA), which shows increased expression of this gene in various tumor types including NSCLC, bladder, breast, cervical, cholangiocarcinoma, colon, and esophageal cancers [22]. This finding aligns with reports in lung squamous cell carcinoma [23], bladder cancer [24], cervical cancer [7], and oral squamous cell carcinoma [25]. S100A7 is further known for its prognostic value, being associated with poor outcomes, metastasis, and resistance to immunotherapy [7,24,26,27]. Mechanistically, S100A7 promotes tumor progression through multiple pathways such as AKT, NF-κB, and ERK via interactions with JAB1 and RAGE [28,29]. It also induces epigenetic alterations, impairs mismatch repair systems [22], and promotes angiogenesis through the IGF-1/RAGE/VEGF axis [30], positioning it as a key regulator of malignancy and a promising therapeutic target.

S100A11 was also found to be decreased in urinary exosomes of SCLC patients, supporting prior observations of its tumor-suppressive role in SCLC, colorectal cancer (CRC), and bladder cancer [31,32]. In contrast, S100A11 functions as an oncogene in NSCLC, where it enhances tumor proliferation [33,34]. Its reduced exosomal levels, despite potentially unchanged serum concentrations, may result from selective exosomal exclusion in SCLC, highlighting the need to consider compartment-specific biomarker profiles.

Furthermore, the study showed that S100A16 was significantly downregulated in SCLC urinary exosomes, consistent with findings in CRC and oral cancers, where reduced level promotes proliferation and EMT through pathways like JNK/p38 MAPK [35,36]. However, this contrasts with studies in lung adenocarcinoma (LUAD), pancreatic cancer, and osteosarcoma, where S100A16 is upregulated and associated with poor outcomes [37–39]. These differences likely reflect tissue-specific regulatory mechanisms, such as hypomethylation in LUAD and hypermethylation in SCLC, which modulate both expression and exosomal secretion of S100A16 [37].

Additionally, the study found decreased levels of S100A8 and S100A9 in urinary exosomes from SCLC pa-

tients, in contrast to their increased expression in NSCLC and other cancer types [40]. This may reflect a strategy of immune evasion through reduced exosome-mediated immunomodulatory signaling, weakening antitumor responses in SCLC.

In conclusion, the study highlights the diagnostic and mechanistic relevance of S100A6 and other S100 proteins as promising non-invasive biomarkers in SCLC. The demographic stability and strong diagnostic performance of S100A6, especially in a cohort where 81% were in the extensive stage, addresses key limitations of tissue biopsies by offering a non-invasive method for disease monitoring. Stratified abundance patterns across age and sex also support the development of personalized reference intervals.

Several limitations of this pilot study should be acknowledged. First, the relatively small sample size may introduce a risk of model overfitting. Therefore, further validation in large-scale, multi-ethnic, and multi-center independent cohorts is required to confirm the robustness and generalizability of our findings. Second, sex-stratified validation was only performed in healthy individuals, and the diagnostic performance of S100A6 in female patients with SCLC remains unvalidated. Future prospective studies should include female SCLC patients to evaluate its clinical applicability across both sexes. Third, most patients in this study were extensive-stage SCLC; thus, future investigations should focus on limited-stage disease to explore the early diagnostic utility of this biomarker. Finally, although we focused on protein abundance profiles, further studies are warranted to elucidate the underlying molecular mechanisms and regulatory pathways, which will help fully define the clinical potential of these biomarkers. Finally, although the study emphasized protein abundance levels, further exploration of molecular mechanisms and regulatory pathways is needed to fully understand the clinical potential of these biomarkers.

Conclusion

In summary, our findings establish urinary exosomal S100 proteins, particularly S100A6, as valuable non-invasive biomarkers for detecting SCLC in male patient. The identification of demographic-specific abundance patterns for other S100 family members also provides crucial baseline information for developing personalized diagnostic and prognostic strategies. This study represents a significant step towards improving early diagnosis and understanding the molecular mechanisms underlying this aggressive malignancy.

Availability of Data and Materials

The datasets used and analyzed during the current study are available from the corresponding authors on reasonable request.

Author Contributions

MZ, LP: Conceptualization; Formal analysis; Funding acquisition; Methodology; Project administration; Resources; Writing—review & editing. WW: Investigation; Methodology; Data curation; Software; Writing—original draft; Writing—review & editing. NL, SW, AA: Investigation; Methodology; Supervision; Writing—review & editing. All authors read and approved the final manuscript. All authors have participated sufficiently in the work to take public responsibility for appropriate portions of the content and agreed to be accountable for all aspects of the work in ensuring that questions related to its accuracy or integrity.

Ethics Approval and Consent to Participate

The study adhered to the standards outlined in the Declaration of Helsinki and was approved by the Ethics Committee of Beijing Shijitan Hospital (No. 5, 2017). All participants provided written informed consent after being informed of the study procedures and potential risks.

Acknowledgment

We are grateful to all volunteers whose urine and tissues donations made this study possible.

Funding

This work was supported by the Beijing Key Laboratory of Urinary Cellular Molecular Diagnostics and Beijing Shijtan Hospital's "14th Five-Year Plan" Leading Talent Training Project (2023LJRCPL).

Conflict of Interest

The authors declare no conflict of interest.

References

[1] Siegel RL, Kratzer TB, Giaquinto AN, Sung H, Jemal A. Cancer statistics, 2025. CA: A Cancer Journal for Clinicians. 2025; 75: 10–45. https://doi.org/10.3322/caac.21871.

[2] Sugumar V, Salunkhe R, Lone H, Ye X, Zhan L, Sun A, *et al*. Retrospective cohort study assessing clinical outcomes of patients with extensive-stage small cell lung cancer treated with and without consolidative thoracic radiotherapy at the Princess Margaret Cancer Centre. BMJ Open. 2025; 15: e093943. https://doi.org/10.1136/bmjopen-2024-093943.

[3] Li L, Zhang Q, Wang Y, Xu C. Evaluating the diagnostic and prognostic value of serum TuM2-PK, NSE, and ProGRP in small cell lung cancer. Journal of Clinical Laboratory Analysis. 2023; 37: e24865. https://doi.org/10.1002/jcla.24865.

[4] Wang T, Liu R. S100 Protein Family in Lung Cancer: an Updated Narrative Review. Cancer Management and Research. 2025; 17: 713–722. https://doi.org/10.2147/CMAR.S508047.

[5] Bresnick AR, Weber DJ, Zimmer DB. S100 proteins in cancer. Nature Reviews. Cancer. 2015; 15: 96–109. https://doi.org/10.1038/nrc3893.

[6] Allgöwer C, Kretz AL, von Karstedt S, Wittau M, Henne-Bruns D, Lemke J. Friend or Foe: S100 Proteins in Cancer. Cancers. 2020; 12: 2037. https://doi.org/10.3390/cancers12082037.

[7] Ning Y, Chen Y, Tian T, Gao X, Liu X, Wang J, *et al*. S100A7 orchestrates neutrophil chemotaxis and drives neutrophil extracellular traps (NETs) formation to facilitate lymph node metastasis in cervical cancer patients. Cancer Letters. 2024; 605: 217288. https://doi.org/10.1016/j.canlet.2024.217288.

[8] Guo Y, Zhang Z, Huang H, Wu Y, Yin L, Zhou Y, *et al*. Targeting S100A8/A9-NCF1 axis in tumor microenvironment to prevent tumor metastasis by self-assembled peptide nanofibers. Molecular Therapy: the Journal of the American Society of Gene Therapy. 2025; 33: 1502–1518. https://doi.org/10.1016/j.ymthe.2025.02.042.

[9] Khan Y, Fatima R, Khan A, Zhang L, Bisht AS, Hussain MS. Liquid Biopsy for Medical Imaging Analysis in Cancer Diagnosis. Current Pharmaceutical Design. 2025; 31: 2635–2650. https://doi.org/10.2174/0113816128371883250310174153.

[10] Jin S, Liu T, Wang W, Li T, Liu Z, Zhang M. Lymphocyte migration regulation related proteins in urine exosomes may serve as a potential biomarker for lung cancer diagnosis. BMC Cancer. 2023; 23: 1125. https://doi.org/10.1186/s12885-023-11567-x.

[11] Li Y, Zhang H, Sun F, Yu C, Jiang S, Yang L. The diagnosis and prognostic value and biological function of annexin A2 in hepatocellular carcinoma: a bioinformatic and experimental study. Integrative Biology: Quantitative Biosciences from Nano to Macro. 2025; 17: zyaf017. https://doi.org/10.1093/intbio/zyaf017.

[12] Cómitre-Mariano B, Segura-Collar B, Vellila-Alonso G, Contreras R, Hernandez-Lain A, Valiente M, *et al*. S100A proteins show a spatial distribution of inflammation associated with the glioblastoma microenvironment architecture. Theranostics. 2025; 15: 726–744. https://doi.org/10.7150/thno.100638.

[13] Hong B, Zhang H, Xiao Y, Shen L, Qian Y. S100A6 is a potential diagnostic and prognostic biomarker for human glioma. Oncology Letters. 2023; 26: 458. https://doi.org/10.3892/ol.2023.14045.

[14] Li L, Pan Y, Mo X, Wei T, Song J, Luo M, *et al*. A novel metastatic promoter CEMIP and its downstream molecular targets and signaling pathway of cellular migration and invasion in SCLC cells based on proteome analysis. Journal of Cancer Research and Clinical Oncology. 2020; 146: 2519–2534. https://doi.org/10.1007/s00432-020-03308-5.

[15] Farooq A, Akyuz EM, Cheah BW, Deen S, Martin SG, Finelli MJ, *et al*. Increased cytoplasmic and nuclear S100A6 expression is associated with improved prognosis in ovarian cancer. BMC Cancer. 2026; 26: 368. https://doi.org/10.1186/s12885-026-15631-0.

[16] Wang P, He Q, Xu Y, Chen Y, Zeng X, Deng K, *et al*. Exosomal PD-L1 in hepatocellular carcinoma: Immune evasion mechanisms, diagnostic value, and strategies for therapeutic targeting. Biomedicine & Pharmacotherapy. 2026; 198: 119268. https://doi.org/10.1016/j.biopha.2026.119268.

[17] He X, Xu X, Khan AQ, Ling W. High Expression of S100A6 Predicts Unfavorable Prognosis of Lung Squamous Cell Cancer. Medical Science Monitor: International Medical Journal of Experimental and Clinical Research. 2017; 23: 5011–5017. https://doi.org/10.12659/msm.904279.

[18] Wang T, Liang Y, Thakur A, Zhang S, Liu F, Khan H, *et al*. Expression and clinicopathological significance of S100 calcium binding protein A2 in lung cancer patients of Chinese Han ethnicity. Clinica Chimica Acta; International Journal of Clinical Chemistry. 2017; 464: 118–122. https://doi.org/10.1016/j.cca.2016.11.027.

[19] Chen X, Ma S, Zeng W, Huang C, Guo J. Overexpression of S100 Calcium-Binding Protein A2 is Associated With Poor Prognosis in Hepatocellular Carcinoma. Cancer Control: Journal of the Moffitt Cancer Center. 2026; 33: 10732748261433283. https://doi.org/10.1177/10732748261433283.

[20] Garcia-Recio S, Hinoue T, Wheeler GL, Kelly BJ, Garrido-Castro AC, Pascual T, *et al*. Multiomics in primary and metastatic breast tumors from the AURORA US network finds microenvironment and epigenetic drivers of metastasis. Nature Cancer. 2023; 4: 128–147. https://doi.org/10.1038/s43018-022-00491-x.

[21] Ma T, Ma J, Wang Y, Kui X, Liu J, Han C, *et al*. Targeting BACH1/PSPH axis suppresses bladder cancer progression and gemcitabine resistance by downregulating S100A2 expression. Biochemical Pharmacology. 2025; 241: 117182. https://doi.org/10.1016/j.bcp.2025.117182.

[22] Peng G, Tsukamoto S, Okumura K, Ogawa H, Ikeda S, Niyonsaba F. A Pancancer Analysis of the Oncogenic Role of S100 Calcium Binding Protein A7 (S100A7) in Human Tumors. Biology. 2022; 11: 284. https://doi.org/10.3390/biology11020284.

[23] Lu H, Huang W, Shen Q, Liu R. Anoikis-Related Genes Signature Contributes to Predicting Prognosis and Response to Immunotherapy in Lung Squamous Cell Carcinoma. Medical Science Monitor. 2026; 32: e951722. https://doi.org/10.12659/msm.951722.

[24] Cai Y, Cheng Y, Wang Z, Li L, Qian Z, Xia W, *et al*. A novel metabolic subtype with S100A7 high expression represents poor prognosis and immuno-suppressive tumor microenvironment in bladder cancer. BMC Cancer. 2023; 23: 725. https://doi.org/10.1186/s12885-023-11182-w.

[25] Sood A, Mishra D, Kharbanda OP, Chauhan SS, Gupta SD, Deo SSV, *et al*. Role of S100 A7 as a diagnostic biomarker in oral potentially malignant disorders and oral cancer. Journal of Oral and Maxillofacial Pathology: JOMFP. 2022; 26: 166–172. https://doi.org/10.4103/jomfp.jomfp_402_20.

[26] Utsumi H, Yagishita S, Kawajiri K, Torasawa M, Kiritani A, Tamura K, *et al*. Identification of poor prognostic factors using circulating extracellular vesicles in durvalumab consolidation therapy for locally advanced non-small cell lung cancer. Lung Cancer. 2025; 208: 108732. https://doi.org/10.1016/j.lungcan.2025.108732.

[27] Zhang T, Yu X, Yang X, Li Y, Li X, Ma L. A Nomogram Based on S100A7 and Clinicopathological Characteristics to Predict the Efficacy of Neoadjuvant Chemotherapy in Breast Cancer: A Retrospective Study. Therapeutics and Clinical Risk Management. 2025; 21: 283–292. https://doi.org/10.2147/tcrm.S508507.

[28] Lu Z, Li Y, Che Y, Huang J, Sun S, Mao S, *et al*. The TGFβ-induced lncRNA TBILA promotes non-small cell lung cancer progression in vitro and in vivo via cis-regulating HGAL and activating S100A7/JAB1 signaling. Cancer Letters. 2018; 432: 156–168. https://doi.org/10.1016/j.canlet.2018.06.013.

[29] Rojas A, Schneider I, Lindner C, Gonzalez I, Morales MA. The RAGE/multiligand axis: a new actor in tumor biology. Bioscience Reports. 2022; 42: BSR20220395. https://doi.org/10.1042/bsr20220395.

[30] Muoio MG, Talia M, Lappano R, Sims AH, Vella V, Cirillo F, *et al*. Activation of the S100A7/RAGE Pathway by IGF-1 Contributes to Angiogenesis in Breast Cancer. Cancers. 2021; 13: 621. https://doi.org/10.3390/cancers13040621.

[31] Hao J, Wang K, Yue Y, Tian T, Xu A, Hao J, *et al*. Selective expression of S100A11 in lung cancer and its role in regulating proliferation of adenocarcinomas cells. Molecular and Cellular Biochemistry. 2012; 359: 323–332. https://doi.org/10.1007/s11010-011-1026-8.

[32] Moravkova P, Kohoutova D, Vavrova J, Bures J. Serum S100A6, S100A8, S100A9 and S100A11 proteins in colorectal neoplasia:

results of a single centre prospective study. Scandinavian Journal of Clinical and Laboratory Investigation. 2020; 80: 173–178. https://doi.org/10.1080/00365513.2019.1704050.

[33] Zheng M, Meng H, Li Y, Shi J, Han Y, Zhao C, *et al*. S100A11 Promotes Metastasis via AKT and ERK Signaling Pathways and Has a Diagnostic Role in Hepatocellular Carcinoma. International Journal of Medical Sciences. 2023; 20: 318–328. https://doi.org/10.7150/ijms.80503.

[34] Wang H, He R, Liu D, He J, Shen Z. S100A11 as an immune-related exosomal driver of colorectal cancer progression: a novel diagnostic biomarker. Frontiers in Oncology. 2025; 15: 1590128. https://doi.org/10.3389/fonc.2025.1590128.

[35] Ou S, Liao Y, Shi J, Tang J, Ye Y, Wu F, *et al*. S100A16 suppresses the proliferation, migration and invasion of colorectal cancer cells in part via the JNK/p38 MAPK pathway. Molecular Medicine Reports. 2021; 23: 164. https://doi.org/10.3892/mmr.2020.11803.

[36] Sapkota D, Bruland O, Parajuli H, Osman TA, Teh MT, Johannessen AC, *et al*. S100A16 promotes differentiation and contributes to a less aggressive tumor phenotype in oral squamous cell carcinoma. BMC Cancer. 2015; 15: 631. https://doi.org/10.1186/s12885-015-1622-1.

[37] Chen D, Luo L, Liang C. Aberrant S100A16 expression might be an independent prognostic indicator of unfavorable survival in non-small cell lung adenocarcinoma. PloS One. 2018; 13: e0197402. https://doi.org/10.1371/journal.pone.0197402.

[38] Hu P, Fei Z, Bai J, Wang Z, Jin Y. *S100A14* Facilitates Pancreatic Cancer Progression via *S100A16*-Mediated *p53* Suppression. Oncology Research. 2026; 34: 24. https://doi.org/10.32604/or.2025.070207.

[39] Xiang YY, Liu JH, Yi X, Luo JY, Yu Y, Yi GL. S100 A16 promotes the progression of osteosarcoma by activating the PI3 K/AKT signaling pathway through ANXA2. Scientific Reports. 2025; 15: 19962. https://doi.org/10.1038/s41598-025-05293-6.

[40] Chen Y, Ouyang Y, Li Z, Wang X, Ma J. S100A8 and S100A9 in Cancer. Biochimica et Biophysica Acta. Reviews on Cancer. 2023; 1878: 188891. https://doi.org/10.1016/j.bbcan.2023.188891.